NEOPLASIA
www.neoplasia.com
Volume 22 Number 7 July 2020 pp. 274-282

Original Research

Molecular mechanisms of Guadecitabine induced FGFR4 down regulation in alveolar rhabdomyosarcomas

Emad Darvishi [a]; Katherine Slemmons [a]; Zesheng Wan [a]; Sheetal Mitra [a]; Xiaogang Hou [a]; Jean Hugues Parmentier [a]; Yong-Hwee Eddie Loh [b]; Lee J. Helman [a,c,*]

[a] Division of Hematology-Oncology, Cancer and Blood Disease Institute, Children's Hospital Los Angeles, Los Angeles, CA, USA [b] USC Libraries Bioinformatics Services, Los Angeles, CA, USA; [c] Keck School of Medicine, University of Southern California, Los Angeles, CA, USA

Abstract

Fibroblast growth factor receptor 4 (FGFR4) aberrant expression and activity have been linked to the pathogenesis of a variety of cancers including rhabdomyosarcomas (RMS). We found that treatment of alveolar rhabdomyosarcoma (aRMS) cells with Guadecitabine (SGI-110), a next-generation DNA methyltransferase inhibitor (DNMTi), resulted in a significant reduction of FGFR4 protein levels, 5 days post treatment. Chromatin immunoprecipitation-sequencing (ChIP-seq) in aRMS cells revealed attenuation of the H3K4 mono-methylation across the FGFR4 super enhancer without changes in tri-methylation of either H3K4 or H3K27. These changes were associated with a significant reduction in FGFR4 transcript levels in treated cells. These decreases in H3K4me1 in the FGFR4 super enhancer were also associated with a 240-fold increase in KDM5B (JARID1B) mRNA levels. Immunoblot and immunofluorescent studies also revealed a significant increase in the KDM5B protein levels after treatment in these cells. KDM5B is the only member of KDM5 (JARID1) family of histone lysine demethylases that catalyzes demethylation of H3K4me1. These data together suggest a pleiotropic effect of DNMTi therapy in aRMS cells, converging to significantly lower FGFR4 protein levels in these cells.

Neoplasia (2020) 22 274–282

Keywords: Fibroblast growth factor receptor 4 (FGFR4), Alveolar rhabdomyosarcoma (aRMS), Guadecitabine (SGI-110), Epigenetic marks, Histone lysine demethylase 5B (KDM5B)

Introduction

Aberrant DNA methylation in cancer cells that results in activation of oncogenes and silencing of tumor-suppressor genes introduces epigenetic modifiers as a promising therapeutic target for cancer treatment. Hypermethylation of five to ten percent of promoter CpG islands in most cancers results in silencing of many critical tumor suppressor genes [1,2]. The reversible nature of epigenetic alterations present new opportunities to utilize DNA methylation inhibitors such as 5-azacytidine (azacitidine), 5-aza-2′-deoxycytidine (decitabine) and guadecitabine (SGI-110) for epigenetic therapy of cancer [3]. These drugs incorporate into DNA and trap DNA methyltransferases (DNMTs) in the form of a covalent protein–DNA adduct that in turn alters DNA and histone epigenetic profiles, reprogram tumor cells to a more normal-like state by affecting multiple pathways and sensitize them to chemotherapy and immunotherapy [4].

SGI-110 treatment in hepatocellular carcinoma cells resulted in inhibition of cell growth and delayed tumor growth in mouse xenograft models [5,6]. The preclinical *in vivo* findings also demonstrated the clinical potential of SGI-110 for reducing lung tumor burden through reprogramming the epigenome [7]. SGI-110 treatment has also been effective in decreasing pancreatic ductal adenocarcinoma cell viability and improved their response to the chemotherapeutic agent, Irinotecan [8]. Apart from its clinical progress as a single agent in patients with hematologic malignancies, SGI-110 has presently gained significant interest in combinatorial

Abbreviations: FGFR4, fibroblast growth factor receptor 4, aRMS, alveolar rhabdomyosarcoma, eRMS, embryonal rhabdomyosarcoma, DNMTi, DNA methyltransferase inhibitor, ChIP-seq, Chromatin immunoprecipitation-sequencing, TSS, transcription start site

* Corresponding author.
e-mail address: lhelman@chla.usc.edu (L.J. Helman).

https://doi.org/10.1016/j.neo.2020.05.001

therapies and as a priming agent in solid tumors and is being evaluated in phase 1/2 clinical trials for various solid tumors [9].

In the process of investigating SGI-110 growth inhibitory mechanisms of action in rhabdomyosarcomas (RMS), we noticed a dramatic drug related suppression of fibroblast growth factor receptor 4 (FGFR4) protein levels in both fusion-negative embryonal rhabdomyosarcoma (eRMS) and fusion positive alveolar rhabdomyosarcomas (aRMS). FGFR4 encodes a member of the FGFR family of receptor tyrosine kinases (RTK) that affects diverse cellular processes, including the regulation of cell proliferation, differentiation, migration, metabolism, and bile acid biosynthesis [10–12]. FGFR aberrations have been identified in a variety of disorders including myeloproliferative syndromes, lymphomas, prostate, ovarian and breast cancers as well as other malignant diseases [11–13]. In rhabdomyosarcoma, FGFR4 overexpression at the mRNA and protein levels especially in PAX3-FOXO1-positive aRMS is associated with advanced-stage cancer and lower overall survival [14–16]. Moreover, two activating mutations in FGFR4 tyrosine kinase domain have been identified in 7.5% of primary human RMS tumors [16,17]. In aRMS, genetic depletion of FGFR4 has been shown to inhibit proliferation *in vitro* and reduce proliferation and lung metastasis *in vivo* [16]. In eRMS, FGFR4 loss-of-function reduced cell proliferation *in vitro* and xenograft formation *in vivo*, while in aRMS, it diminished cell survival *in vitro* [18]. Ectopic expression of a constitutively active mutant of FGFR4 has been shown to be involved in the development and progression of aRMS [19].

The important role of the FGFR4 encouraged us to study the mechanisms of SGI-110 induced FGFR4 down regulation in aRMS. Our results, herein, demonstrate that SGI-110 leads to down regulation of FGFR4 at the transcript level via a marked attenuation of the H3K4 mono-methylation across the FGFR4 super enhancer that is associated with upregulation of histone lysine demethylase, KDM5B, in aRMS.

Materials and methods

Cell culture and chemicals

RH30, RH41 and RD cell lines, provided by TJ. Triche (Children's Hospital Los Angeles) and authenticated by short tandem repeat (STR) testing to ensure the identity of the cell lines, were cultured in RPMI-1640 media supplemented with 2 mM l-glutamine, 100U/mL penicillin, 100 μg/mL streptomycin and 10% fetal bovine serum (Sigma–Aldrich, St Louis, MO) and maintained in a humidified incubator containing 5% CO_2 at 37 °C. Guadecitabine (SGI-110) was purchased from MedChemExpress (cat. # HY-13542).

Measurement of cellular proliferation

RH30, RH41 and RD cells were plated at 2000 cells/well in 96-well plates (CytoOne, USA Scientific, Inc) and kept overnight in a humidified incubator containing 5% CO_2 at 37 °C. Next day, cells were treated with the indicated concentrations of SGI-110 and cellular proliferation rate was monitored in an IncuCyte S3 live cell analysis system (Essen BioScience, Ann Arbor, MI, USA) for 8–9 days. SGI-110 stock solution of 5 mM was prepared in fresh molecular biology-grade DMSO. All proliferation studies were performed at least three times.

Cell cycle analysis by BrdU incorporation assay

The cell cycle analysis of control and SGI-110 treated cells was performed using an APC-BrdU flow kit (BD Bioscience Pharmingen, cat. #552598) according to the manufacturer's instructions. Briefly, drug-treated RH30 and RH41 cells (500 nM for 5 days) were labelled with 10 μM BrdU added to the medium for 1 hour. The cells were then fixed, permeabilized, and treated with DNase (300 μg/mL for 1 hour at 37 °C), stained with APC-conjugated monoclonal anti-BrdU antibody, 7-AAD reagent (Overnight at 4 °C), and analyzed on a BD LSR II (BD Biosciences, San Jose, CA) for APC and 7-AAD fluorescent dyes, respectively. In total, 10,000 events were counted for a sample.

Real-Time RT-PCR quantification

RNA was isolated from RH30 and RH41 cell lines treated with the indicated concentrations of SGI-110 for 5 days using the RNeasy plus mini kit (cat #74134) as recommended by the manufacturer. cDNA was generated using the iScript select cDNA synthesis kit (cat #1708896). Quantitative PCR was done using a QuantStudio3 real-time PCR system (Applied Biosystems, CA). For each primer set, reactions were conducted in triplicate using the PowerUp SYBR Green Master Mix (cat. # A25741) according to the instructions of the manufacturer and the following primers: forward – 5′ AAA CCA GCA ACG GCC GCC TG 3′ and reverse – 5′ GTC GAG GTA CTC CTC AGA GAC 3′ (FGFR4); forward – 5′ GAG AGA CCC TCA CTG CTG 3′ and reverse – 5′ GAT GGT ACA TGA CAA GGT GC 3′ (GAPDH). Reactions were initiated with a 10 min incubation at 95 °C followed by 40 cycles at 95 °C for 15 s and 60 °C for 60 s. Relative values of gene expression were calculated with untreated samples as control, and normalized to levels of GAPDH (Glyceraldehyde 3-phosphate dehydrogenase), according to the 2(-Delta Delta C(T)) Method [20].

ChIP-sequencing and data analysis

ChIP-seq was performed as described preciously [21] with some modifications. Briefly, RH30 cells were incubated with SGI-110 (500 nM) or DMSO for 5 days. Cells were then fixed for 8 minutes with 1% formaldehyde and sheared using Bioruptor PLUS Sonicator (Diagenode, Denville, NJ, USA) combined with the bioruptor water cooler at high power setting to achieve chromatin fragmented to a range of 200–600 bp. Immunoprecipitation of sheared chromatin was performed with antibodies against H3K4me1 (Active Motif, cat #39297), H3K4me3 (Active Motif, cat #39159) and H3K27me3 (Active Motif, cat #39155) overnight at 4 °C. DNA purifications were performed with the ChIP-IT High Sensitivity kit (Active Motif, cat #53040). Libraries were prepared from ChIP and Input DNAs using Illumina TruSeq ChIP Library Prep Kit (cat # IP-202–1012) and size selected by following the manufacturer's instructions to obtain a 250–300 bp size-range of DNA fragments. The resulting libraries were then sequenced as paired-end 150-mers on an Illumina NextSeq500 platform. 30,000,000 unique reads were generated per sample. ChIP-seq data processing was performed using Partek Flow (Partek Inc.) All reads were filtered to retain only those with mean base quality score > 20 and duplicate reads were removed. Filtered reads were mapped to reference genome (hg38) using STAR, allowing uniquely-mapped alignments only and peaks were called using MACS2 [22].

Immunoblotting

Cell lysates were prepared in RIPA buffer supplemented with protease/phosphatase inhibitor cocktail (Thermo Fisher Scientific, Waltham, MA, USA). Protein lysates (25–35 μg/lane), as determined by BCA protein assay (Life Technologies), were then separated by SDS-PAGE (NuPAGE; 4%–12% Bis-Tris gels; Invitrogen) and transferred on to a nitrocellulose membrane that was probed with anti-FGFR4 (Cell Signaling Technology, cat. #8562), anti-IGF-1Rβ (Cell Signaling Technology, cat. #9750), anti-MYOD1 (Cell Signaling Technology, cat. # 13812), anti-FOXO1 (Cell Signaling Technology, cat. #2880) and anti-β-Actin (Cell Signaling Technology, cat. #4967) primary antibodies followed by anti-rabbit IgG, HRP-

linked secondary antibody (Cell Signaling Technology, cat. #7074) before detection using an iBright CL1000 imaging system (Thermo Fisher Scientific, MA, USA). iBright analysis software was used for quantification of the intensity of bands of interest.

Immunocytochemistry

After sterilization and coating with Poly-L-Lysine (Sigma), cover slips were placed in 6-well plate and 50,000 cells (RH30 and RH41) in 2 ml of RPMI were plated in each well overnight. The medium was aspirated and the cells were treated with DMSO (control) or SGI-110 (500 nM and/or 700 nM) for 5 days, fixed in 3.7% formaldehyde for 15 min and permeabilized for 10 min in 0.25% Triton X-100. To reduce nonspecific background staining, cells were incubated with blocking buffer (1% BSA in TBST). After 1 hour, cells were labeled with anti-KDM5B (1:100 dilution; Cell signaling, cat. #3273) primary antibody overnight followed by Cy3-conjugated goat anti-rabbit (111-165-045; Jackson ImmunoResearch, West Grove, PA) secondary antibody for another 2 h in the dark at room temperature. Coverslips were then mounted in antifade reagent (Invitrogen) containing DAPI to stain nuclei and imaged on a Leica microscope (DMI6000B, Leica, Wetzlar, Germany) using a 20×/0.70 air objective at room temperature. ImageJ was used for quantification of fluorescence intensity in each image.

Statistical analysis

Results were expressed as the mean þ SD or mean þ SEM. Comparisons between means were made by Student's *t*-test. The difference was considered to be statistically significant when $P < 0.05$.

Results

SGI-110 inhibits cellular proliferation and down regulates FGFR4 protein levels in rhabdomyosarcomas

To investigate the growth inhibitory effect of SGI-110 in rhabdomyosarcomas, we treated aRMS (RH30 and RH41) and eRMS (RD) cells with two different concentrations of the compound and cell proliferation rate was monitored for 8–9 days post treatment in an IncuCyte live cell analysis system. As shown in Fig. 1A, treatment of RD cells with 500 nM and 700 nM SGI-110 caused a statistically significant decrease in cellular proliferation rate of 27.9 þ 0.6% and 36.6 þ 0.7% respectively, compared to the untreated control. Treatment of aRMS cells with the same doses of SGI-110 showed more sensitivity to the drug with a statistically significant decrease of 45.3 þ 0.9% and 54.4 þ 0.7% (RH30 cells) and 72.7 þ 4.7% and 76.4 þ 4.0% (RH41 cells) in cellular proliferation rate, respectively. These data demonstrate that SGI-110 inhibits cell proliferation more effectively in fusion-positive RMS (*i.e.,* RH30 and RH41) than in fusion-negative RMS (*i.e.,* RD). Flow cytometry cell cycle analysis revealed a statistically significant increase in the number of cells in the S-phase in both RH30 (56.5 þ 0.5% compared to 41.5 þ 1.5% in untreated cells) and RH41 (23.8 þ 0.2% compared to 16.3 þ 0.4% in untreated cells) cells 5 days post SGI-110 treatment. Cell accumulation in S-phase of the cell cycle with a significant decrease in the number of cells in G1-phase is indicative of DNA synthesis blockade associated with SGI-110 treatment in aRMS (Supplementary Fig. 1).

Immunoblot analysis of the total cell extracts from drug treated cells indicated a significant reduction in FGFR4 protein levels in aRMS (Fig. 1C & D) and eRMS (Supplementary Fig. 2), 5 days post treatment. However, there were no significant differences between the two doses of SGI-110 used in aRMS (Fig. 1D). RNA-seq data analysis of the RH30 cells treated with 500 nM SGI-110 for 5 days also revealed a statistically significant decrease (Fold change: 0.40, *P*-value: 4.38E-71) in transcript levels of FGFR4 (Supplementary table 1). While FGFR4 is expressed in both aRMS and eRMS cells, it is significantly overexpressed in aRMS tumors. We therefore, focused our studies on exploring molecular mechanisms of SGI-110 induced FGFR4 down regulation in aRMS. As shown in Fig. 1C, we could not detect any significant reductions in the PAX3-FOXO1 and its downstream targets MYOD1 and IGF-1R protein levels in SGI-110 treated RH30 and RH41 cells indicating that SGI-110 induced FGFR4 down regulation is not a downstream effect of PAX3-FOXO1 suppression by SGI-110 in the fusion-positive rhabdomyosarcomas.

SGI-110 attenuates the active enhancer mark, H3K4me1, at the FGFR4 locus and is associated with decreased transcript levels

SGI-110 is a second-generation DNA hypomethylating prodrug whose active metabolite is the well-characterized drug decitabine. This dinucleotide exerts its anticancer activities through gene-specific and global hypomethylation both *in vitro* and in animal model systems [23]. Given that, we hypothesized that SGI-110 may down regulate FGFR4 protein levels through epigenetic alterations at the regulatory elements of FGFR4 locus.

To gain insight into epigenetic mechanisms of FGFR4 down regulation by SGI-110, we investigated the status of the active (*i.e.,* H3K4me1 and H3K4me3) and repressive (*i.e.,* H3K27me3) histone marks across the FGFR4 locus by sequencing DNA enriched by chromatin immunoprecipitation (ChIP-seq) in a fusion-positive RMS cell line, RH30, in the presence of either DMSO (control) or SGI-110. As shown in Fig. 2A, SGI-110 treatment led to the noticeable attenuation of the H3K4 mono-methylation at the FGFR4 super enhancer compared to the untreated control while tri-methylation of H3K4 that is an active promoter mark was not altered. We could not detect any changes in the H3K27 tri-methylation levels after drug treatment (Fig. 2A). It is noteworthy that H3K4me1 peaks across IGF-1R and MYOD1 loci, two downstream targets of PAX3-FOXO1 in aRMS, did not show any noticeable differences between SGI-110-treated and untreated control (Supplementary Fig. 3) that was in accordance with our IGF-1R and MYOD1 immunoblot analysis in Fig. 1C.

Using real-time RT-PCR to measure the transcript abundance of FGFR4 gene, we could detect a statistically significant reduction of 36.9 þ 4.6% and 33.5 þ 5.6% in FGFR4 mRNA levels in RH30 cells exposed to 500 nM and 700 nM SGI-110 for 5 days compared with the untreated control, respectively. A statistically significant decrease of 25.0 þ 6.4% and 35.9 þ 10.9% in FGFR4 transcript levels has also been observed in RH41 cell line, post treatment (Fig. 2B). These results are in agreement with our hypothesis of the importance of epigenetic alterations caused by SGI-110 in modulation of FGFR4 transcript levels and showed that SGI-110 exerts its inhibitory effects on FGFR4 mRNA levels, at least in part, through attenuation of its active enhancer mark (*i.e.,* H3K4me1), in aRMS.

Upregulation of KDM5B by SGI-110 results in a global decrease in the H3K4 mono-methylation levels in aRMS

Global distribution of the active histone modification peaks around the transcription start sites (TSSs) of all reference genes in RH30 cells revealed a noticeable genome-wide attenuation of the mono-methylation of lysine 4 on histone 3 as shown by the stronger red signal in DMSO treated controls compared with SGI-110 treated samples (Fig. 3A, left). However, global tri-methylation of H3K4 at the TSSs of most genes remained unchanged, post treatment (Fig. 3A, right). This observation indicates that SGI-110 may specifically upregulate the enzymes that remove mono-

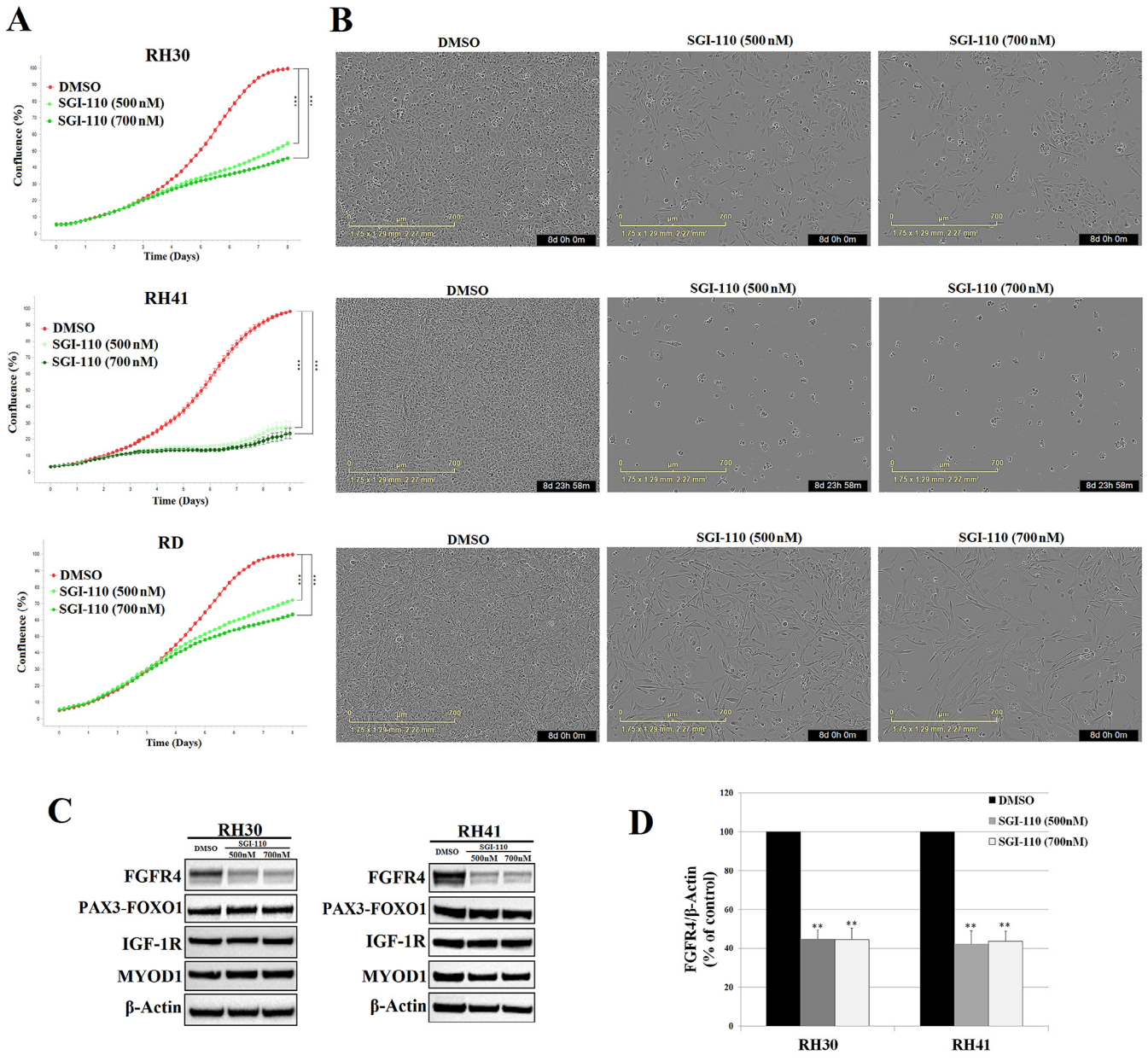

Fig. 1. SGI-110 inhibits cell proliferation more effectively in aRMS than eRMS cells (A) Cell lines were exposed to the indicated concentrations of SGI-110 and cellular proliferation rate was monitored in an IncuCyte S3 live cell analysis system for 8–9 days. Data represent the mean þ SEM of a representative experiment. $^{***}P < 0.001$ versus control (*i.e.,* DMSO). (B) Representative images of DMSO, 500 nM and 700 nM SGI-110 treated RMS cells at day 8. Scale bar = 700 µm. (C) Immunoblot of the total RH30 and RH41 cell extracts treated with the indicated concentrations of SGI-110 or DMSO (control) for 5 days, probed with antibodies against FGFR4, FOXO1, IGF-1R and MYOD1. β-Actin used as a loading control. (D) Densitometric analysis of the immunoblot in C using iBright Analysis Software. Results are the means þ SD pooled from three independent experiments, ** $P < 0.01$ versus untreated controls (*i.e.,* DMSO).

methyl group from the histone H3 lysine K4 in aRMS. In humans, 27 histone lysine demethylases with unique substrate specificities have been identified that can discriminate between different lysine residues and their degree of methylation. KDM1A (LSD1) and KDM1B (LSD2) from the LSD demethylase family and KDM5B (JARID1B) and RIOX1 (NO66) from the Jumonji C demethylase family are able to catalyze demethylation of H3K4me1 [24–26]. RNA-seq data analysis of the RH30 cells treated with 500 nM SGI-110 for 5 days revealed a statistically significant 240-fold increase in transcript levels of KDM5B (JARID1B), while there were no changes in expression levels of the other lysine demethylases, post treatment (Table 1). Furthermore, ChIP-seq analysis demonstrated a significant increase in the active promoter mark, H3K4me3, at the TSS of KDM5B, while tri-methylation of H3K4 at the TSS of KDM1A and KDM1B for instance, remained unchanged, post treatment of RH30 cells (Fig. 3B and supplementary Fig. 4). Immunoblot analysis of the total cell extracts revealed a significant increase in KDM5B protein levels in drug-treated RH30 and RH41 cells (Fig. 4A). These results were further confirmed by immunostaining and imaging of KDM5B protein in aRMS cells treated with or without SGI-110 for 5 days. As shown in Fig. 4B, in the presence of the compound, we observed a significant increase in KDM5B protein levels in the nucleus of the treated cells compared to untreated controls. These observations demonstrate that SGI-110 specifically upreg-

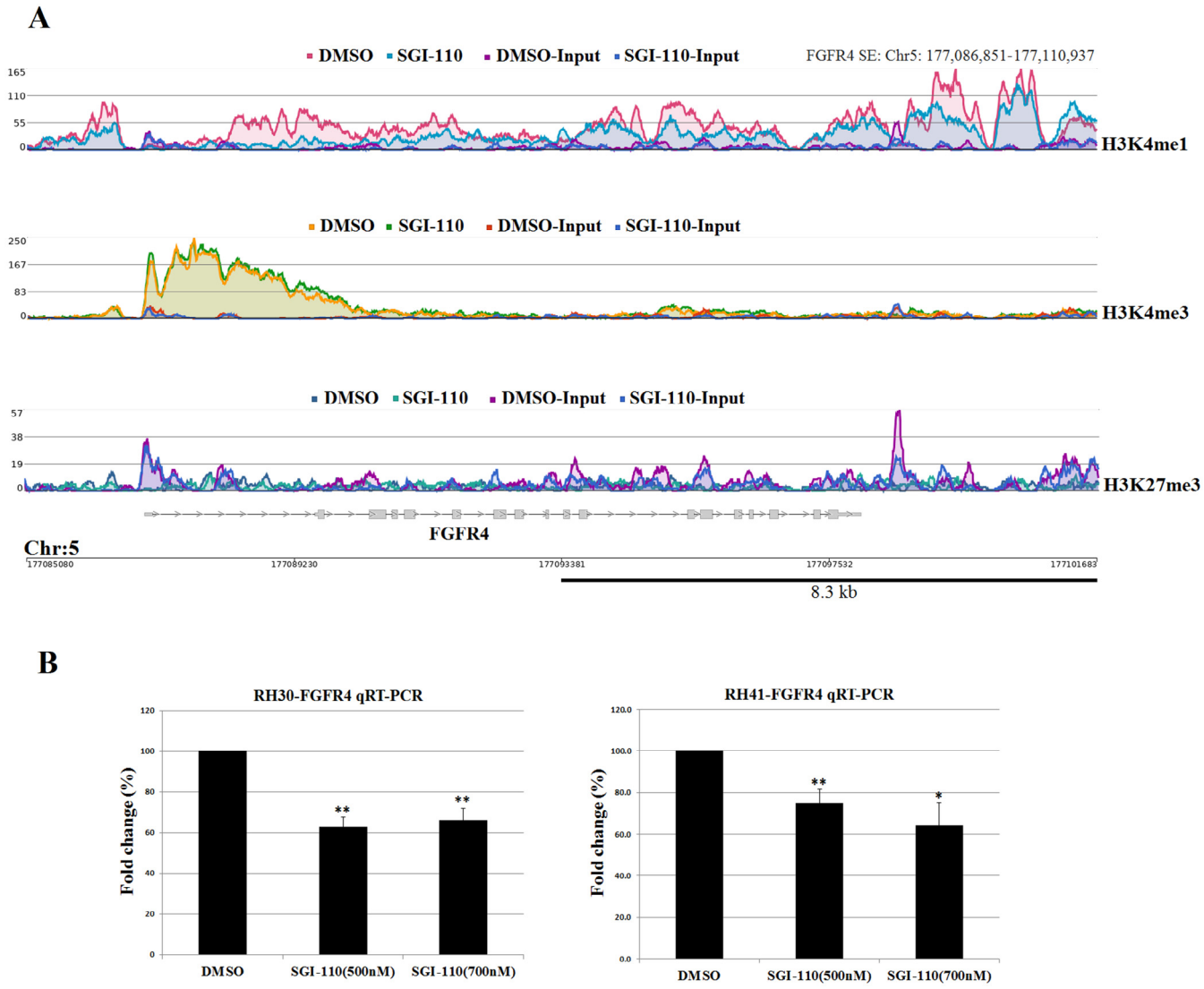

Fig. 2. Attenuation of active enhancer mark (H3K4me1) across the FGFR4 locus and its mRNA levels by SGI-110 (A) Chromatin immunoprecipitation was performed using the ChIP-IT® High Sensitivity Kit (Cat. #53040) with chromatin from RH30 cells, before and after treatment with 500 nM SGI-110 for 5 days using antibodies against H3K4me1 (Active Motif, cat. #39297), H3K4me3 (Active Motif, cat. #39159) and H3K27me3 (Active Motif cat. #39155). ChIP DNAs were sequenced on the Illumina Nextseq 500 sequencer and 30 million sequence tags were mapped to identify H3K4me1, H3K4me3 and H3K27me3 binding sites across the FGFR4 super enhancer (SE) on chromosome 5. (B) Real-time RT-PCR was used to determine the expression levels of FGFR4 gene. Gene expression was normalized to that of the Glyceraldehyde 3-phosphate dehydrogenase (GAPDH) gene. The results indicate significant reductions in the amounts of FGFR4 mRNAs in the presence of SGI-110 relative to DMSO treated control in both RH30 and RH41 cell lines. Reactions were conducted in triplicate and results were expressed as the mean þ SD, $^{*}P < 0.05$, $^{**}P < 0.01$.

ulates histone lysine demethylase, KDM5B that likely contributes to genome-wide demethylation of H3K4me1, in aRMS.

Discussion

Fibroblast growth factor receptors (FGFRs) play a critical role in tumorigenesis and cancer progression through increased cell proliferation, metastasis, and survival [27,28]. Altered expression, mutation, chromosomal rearrangement and abnormal splicing of the FGFR4 gene have been observed in many cancers including rhabdomyosarcomas, making it an attractive therapeutic target. Several compounds to target FGFR4 are in preclinical development or in the early phase of clinical trials [29].

Treatment of cells with the DNA methyltransferase inhibitor, SGI-110, suppressed the expression of FGFR4 in both eRMS and aRMS, but was a more potent growth inhibitor in aRMS cells. Given the pleiotropic effects of epigenetic modifiers such as SGI-110 on the gene expression profile of cells, we hypothesized that SGI-110 mediated FGFR4 down regulation can be modulated at transcription levels through alterations of active and/or repressive histone marks across the FGFR4 locus.

The aRMS specific fusion transcription factor, PAX3–FOXO1, has previously been shown to bind to and activate the expression of the FGFR4 [30]. The mechanism of this activation has been shown to occur through induction of active enhancer and promoter-associated histone marks which in turn activate its transcription in fusion-positive RMS [21]. In the absence of the SGI-110, FGFR4 harbors active enhancer (H3K4me1) and promoter (H3K4me3) marks, as reported previously [21]. However, a significant reduction in the active enhancer mark was observed across the FGFR4 locus post SGI-110 treatment while we could

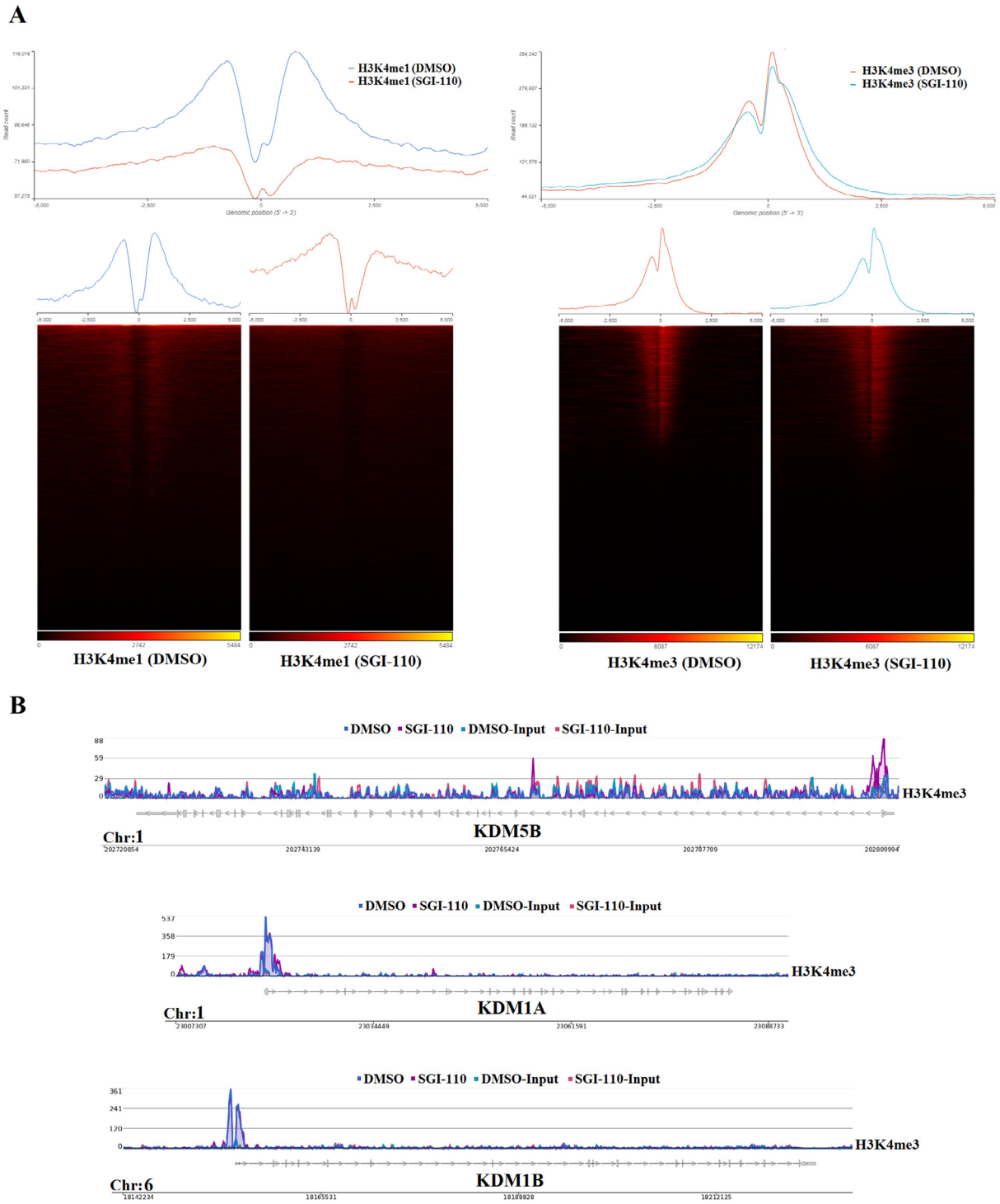

Fig. 3. Genome-wide attenuation of H3K4me1 is linked to the KDM5B upregulation by SGI-110 in aRMS (A) Genome-wide distribution of the active enhancer (H3K4me1, left) and the active promoter (H3K4me3, right) marks is shown in the range of −5000 bp to + 5000 bp from transcription start site (TSS) of all reference genes, in RH30 cells with or without SGI-110 treatment for 5 days. (B) Genome browser tracks of H3K4me3 binding sites across KDM5B (JARID1B), KDM1A (LSD1) and KDM1B (LSD2) loci on chromosomes 1 and 6 following DMSO or SGI-110 treatment for 5 days in RH30 cells. A noticeable increase in the active promoter mark, H3K4me3, at the TSS of KDM5B, was observed after drug treatment.

not detect noticeable changes in tri-methylation levels of H3K4 and H3K27 at this locus. Histone marks have diverse functions in gene regulation. However, these changes and effects are not fully understood. It has been reported that different histone marks recruit specific effector proteins important for each stage of the transcription cycle. The presence of several different domains in these effector proteins that interact with specific histone marks enables them to recognize those histone marks to serve critical modulatory functions in gene expression [31,32]. Specific attenuation of H3K4 mono-methylation at the FGFR4 super enhancer post SGI-110 treatment associated with a significant reduction in FGFR4 transcript

Table 1. The expression fold change of 27 histone lysine demethylases in SGI-110 treated RH30 cells relative to untreated controls.

Gene symbol	Description	*p value*	FDR	Fold change
KDM5B	Lysine demethylase 5B	2.6E-34	7.8E-33	240.687935
HR	HR lysine demethylase and nuclear receptor corepressor	3.7E-76	4.32E-74	3.37075988
KDM7A	Lysine demethylase 7A	3.52E-36	1.15E-34	2.845134656
KDM4D	Lysine demethylase 4D	0.000131	0.000426	1.79380289
KDM2A	Lysine demethylase 2A	1.87E-66	1.67E-64	1.743015431
KDM3A	Lysine demethylase 3A	3.55E-54	2.24E-52	1.607644584
PHF8	PHD finger protein 8	1.21E-29	2.9E-28	1.555862926
KDM1B	Lysine demethylase 1B	5.78E-11	4.1E-10	1.469735662
KDM2B	Lysine demethylase 2B	8.65E-14	7.98E-13	1.403889049
KDM5A	Lysine demethylase 5A	1.65E-10	1.12E-09	1.300652404
KDM5C	Lysine demethylase 5C	6.91E-08	3.52E-07	1.220667349
KDM6A	Lysine demethylase 6A	0.003038	0.007816	1.151442116
KDM1A	Lysine demethylase 1A	0.001537	0.00417	1.116776185
KDM3B	Lysine demethylase 3B	0.00063	0.001834	1.091826343
UBE2B	Ubiquitin conjugating enzyme E2B	0.228322	0.343853	1.067270695
UTY	Ubiquitously transcribed tetratricopeptide repeat containing, Y-linked	0.536296	0.661646	1.054652928
KDM4B	Lysine demethylase 4B	0.693467	0.794954	1.018621115
HSF4	Heat shock transcription factor 4	0.946054	0.962164	0.992851548
KDM4A	Lysine demethylase 4A	0.540899	0.665844	0.970823346
KDM6B	Lysine demethylase 6B	0.036541	0.073172	0.90424066
KDM4C	Lysine demethylase 4C	0.252949	0.373169	0.896232082
JMJD1C	Jumonji domain containing 1C	0.021697	0.046091	0.892761087
PHF2	PHD finger protein 2	0.000479	0.001425	0.890569119
KDM5D	Lysine demethylase 5D	0.000757	0.002171	0.843429953
KDM8	Lysine demethylase 8	0.081357	0.145568	0.829360451
RIOX1	Ribosomal oxygenase 1	N/A	N/A	N/A
RIOX2	Ribosomal oxygenase 2	N/A	N/A	N/A

levels underscores the importance of the active enhancer mark, H3K4me1, in regulation of FGFR4 gene expression in aRMS. In a recently published model [33], the loss of binding of CTCF to its hypermethylated insulators in SDH-deficient gastrointestinal stromal tumors (GISTs) allowing aberrant physical interaction between super enhancer and promoter resulted in the marked upregulation of oncogenes such as FGF4 and FGF3. Such models may also explain how hypomethylating agents such as SGI-110 can down regulate oncogenes by altering chromosome topology. Although treatment with DNMTi leading to global gene body DNA demethylation has been also suggested as one of the causes of the oncogene's down regulation [34,35], it has become clear that DNMT inhibitors are able to cause a regional remodeling of chromatin by changing the histone marks independent of their effects on cytosine methylation [36,37] and our data would suggest treatment of aRMS cells with SGI-110 has such effects.

Despite the widely described correlation of different histone marks with genomic regions and state of gene expression, whether and how they are functional in transcription is still controversial [38]. While the role of H3K4me3 in promoting transcription initiation has been extensively reported, not all cellular genes show dependency on H3K4 trimethylation. For instance, loss of this active promoter mark at expressed CpG island-associated genes in embryonic stem cells did not lead to reduced transcription [39]. In addition, reduction in global levels of H3K4 methylation using siRNA against core subunits of mammalian H3K4 methyltransferase complexes, does not affect the steady-state expression of every gene [40,41]. Hence, more detailed studies are necessary to further reveal the potential function of these histone marks in regulation of transcription of different genes in different cell contexts.

The observed genome-wide attenuation of the H3K4 monomethylation but not tri-methylation, post treatment of RH30 cells and the observed SGI-110 mediated upregulation of the specific histone lysine demethylase, KDM5B, the only member of KDM5 (JARID1) family of histone lysine demethylases that catalyzes demethylation of H3K4me1 [25,26], implicates KDM5B in the removal of the active enhancer mark, H3K4me1 in aRMS. It's been already shown that hypomethylation of promoter DNA by SGI-110 results in upregulation of genes including tumor suppressors [6] and we believe KDM5B promoter demethylation by SGI-110 leads to its upregulation in aRMS cells as can be clearly seen by a noticeable increase in the active promoter mark (*i.e.,* H3K4me3) at KDM5B transcription start site, post treatment.

In summary, these data suggest that treatment of aRMS cells with a DNMTi, SGI-110, leads to a marked decrease in FGFR4 protein levels by a decrease in FGFR4 transcription via a marked attenuation of the H3K4 mono-methylation across the FGFR4 super enhancer that most likely results from an increase in the histone lysine demethylase, KDM5B protein levels apparently through increased H3K4me3 at the TSS of this gene. These data together suggest a pleiotropic effect of DNMTi therapy in aRMS cells, converging to significantly lower FGFR4 protein levels in these cells.

Acknowledgments

We would like to acknowledge the SC2, FACS9 and confocal microscopy core facilities at Children's Hospital Los Angeles for technical assistance.

Funding

The study was supported by endowment funds for sarcoma research to LJH.

Declaration of competing interest

The authors declare that they have no known competing financial interests or personal relationships that could have appeared to influence the work reported in this paper.

Appendix A. Supplementary data

Supplementary data to this article can be found online at https://doi.org/10.1016/j.neo.2020.05.001.

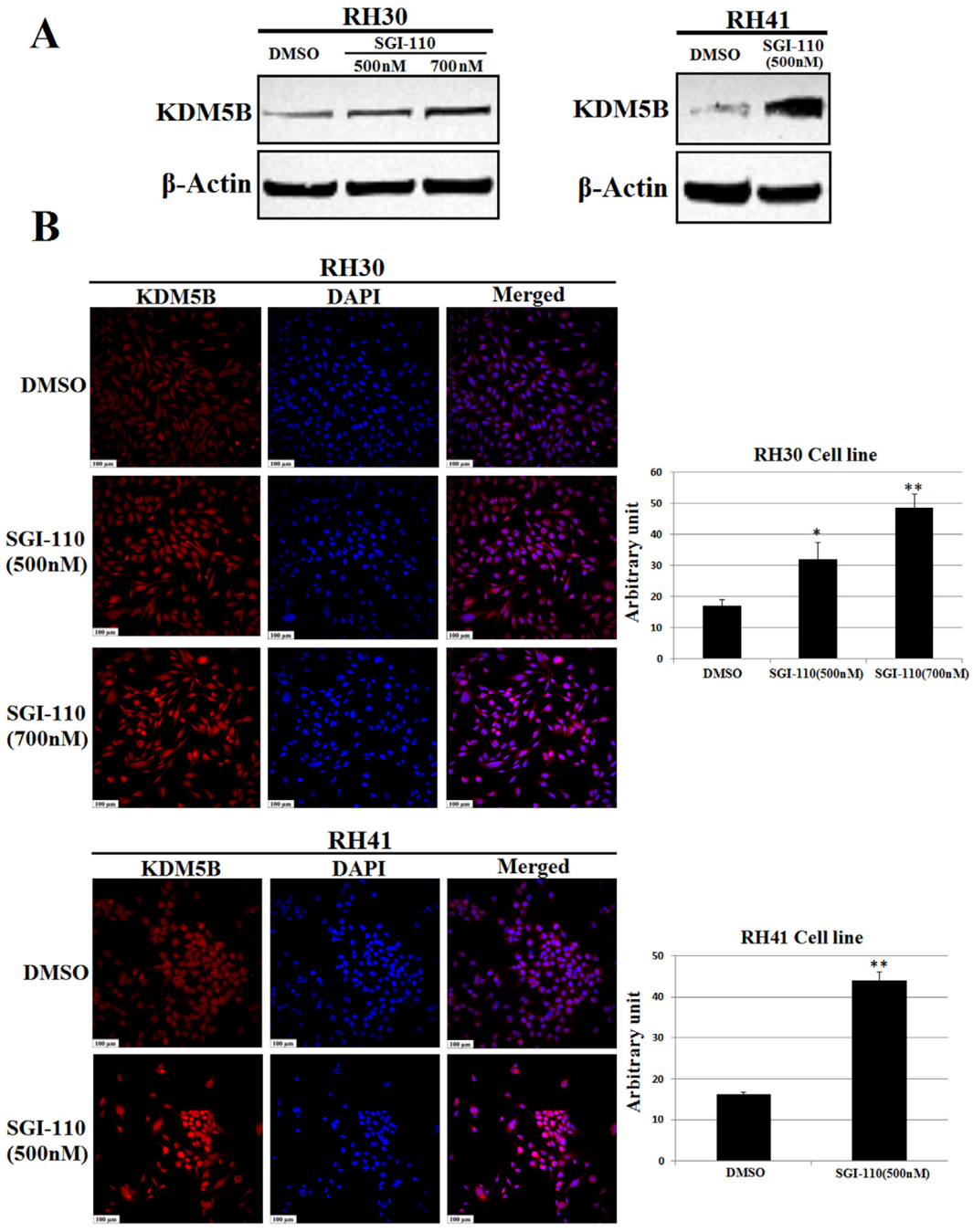

Fig. 4. SGI-110 upregulates histone lysine demethylase, KDM5B, in aRMS (A) Immunoblot of the total RH30 and RH41 cell extracts treated with the indicated concentrations of SGI-110 or DMSO (control) for 5 days, probed with antibody against KDM5B. β-Actin used as a loading control. (B) Immunofluorescent analysis of RH30 and RH41 cells treated with DMSO or indicated concentrations of SGI-110 for 5 days using anti-KDM5B rabbit primary antibody followed by Cy3-conjugated goat anti-rabbit (red) secondary antibody staining. DAPI was used to stain the nucleus (blue). Scale bar represents 100 μm. ImageJ was used for quantification of fluorescence intensity in each image. Each value is the mean þ SD of at least three analyzed images per condition, $^{*}P < 0.05$, $^{**}P < 0.01$ versus control (*i.e.,* DMSO).

References

1. Taby R, Issa JP. Cancer epigenetics. *CA Cancer J Clin* 2010;**60**:376–92.
2. Baylin SB, Jones PA. A decade of exploring the cancer epigenome - biological and translational implications. *Nat Rev Cancer* 2011;**11**:726–34.
3. Issa JP, Kantarjian HM. Targeting DNA methylation. *Clin Cancer Res* 2009;**15**:3938–46.
4. Sato T, Issa JJ, Kropf P. DNA Hypomethylating Drugs in Cancer Therapy. *Cold Spring Harb Perspect Med* 2017;**7**.
5. Jueliger S, Lyons J, Cannito S, Pata I, Pata P, Shkolnaya M, Lo Re O, Peyrou F, Villarroya F, Pazienza V, Rappa F, Cappello F, Azab M, Taverna P, Vinciguerra M. Efficacy and epigenetic interactions of novel DNA hypomethylating agent guadecitabine (SGI-110) in preclinical models of hepatocellular carcinoma. *Epigenetics* 2016;**11**:709–20.
6. Liu M, Zhang L, Li H, Hinoue T, Zhou W, Ohtani H, El-Khoueiry A, Daniels J, O'Connell C, Dorff TB. Integrative Epigenetic Analysis Reveals Therapeutic Targets to the DNA Methyltransferase Inhibitor Guadecitabine (SGI-110) in Hepatocellular. *Carcinoma* 2018;**68**:1412–28.

7. Tellez CS, Grimes MJ, Picchi MA, Liu Y, March TH, Reed MD, Oganesian A, Taverna P, Belinsky SA. SGI-110 and entinostat therapy reduces lung tumor burden and reprograms the epigenome. *Int J Cancer* 2014;**135**:2223–31.
8. Thakar M, Hu Y, Morreale M. A novel epigenetic modulating agent sensitizes pancreatic cells to a chemotherapy agent. 2018; 13: e0199130..
9. Agrawal K, Das V, Vyas P, HajdÇch M. Nucleosidic DNA demethylating epigenetic drugs - A comprehensive review from discovery to clinic. *Pharmacol Therap* 2018;**188**:45–79.
10. Partanen J, Makela TP, Eerola E, Korhonen J, Hirvonen H, Claesson-Welsh L, Alitalo K. FGFR-4, a novel acidic fibroblast growth factor receptor with a distinct expression pattern. *Embo J* 1991;**10**:1347–54.
11. Eswarakumar VP, Lax I, Schlessinger J. Cellular signaling by fibroblast growth factor receptors. *Cytokine Growth Factor Rev* 2005;**16**:139–49.
12. Lang L, Teng Y. Fibroblast Growth Factor Receptor 4 Targeting in Cancer: New Insights into Mechanisms and Therapeutic Strategies. Cells; 2019: 8..
13. Helsten T, Elkin S, Arthur E, Tomson BN, Carter J, Kurzrock R. The FGFR landscape in cancer: analysis of 4,853 tumors by next-generation sequencing. *Clin Cancer Res* 2016;**22**:259–67.
14. Khan J, Wei JS, Ringner M, Saal LH, Ladanyi M, Westermann F, Berthold F, Schwab M, Antonescu CR, Peterson C, Meltzer PS. Classification and diagnostic prediction of cancers using gene expression profiling and artificial neural networks. *Nat Med* 2001;**7**:673–9.
15. Davicioni E, Finckenstein FG, Shahbazian V, Buckley JD, Triche TJ, Anderson MJ. Identification of a PAX-FKHR gene expression signature that defines molecular classes and determines the prognosis of alveolar rhabdomyosarcomas. *Cancer Res* 2006;**66**:6936–46.
16. Taylor JGt, Cheuk AT, Tsang PS, Chung JY, Song YK, Desai K, Yu Y, Chen QR, Shah K, Youngblood V, Fang J, Kim SY, Yeung C, Helman LJ, Mendoza A, Ngo V, Staudt LM, Wei JS, Khanna C, Catchpoole D, Qualman SJ, Hewitt SM, Merlino G, Chanock SJ, Khan J. Identification of FGFR4-activating mutations in human rhabdomyosarcomas that promote metastasis in xenotransplanted models. J Clin Invest 2009;119:3395-407.
17. Shukla N, Ameur N, Yilmaz I, Nafa K, Lau CY, Marchetti A, Borsu L, Barr FG, Ladanyi M. Oncogene mutation profiling of pediatric solid tumors reveals significant subsets of embryonal rhabdomyosarcoma and neuroblastoma with mutated genes in growth signaling pathways. *Clin Cancer Res* 2012;**18**:748–57.
18. Crose LE, Etheridge KT, Chen C, Belyea B, Talbot LJ, Bentley RC, Linardic CM. FGFR4 blockade exerts distinct antitumorigenic effects in human embryonal versus alveolar rhabdomyosarcoma. *Clin Cancer Res* 2012;**18**:3780–90.
19. Marshall AD, van der Ent MA, Grosveld GC. PAX3-FOXO1 and FGFR4 in alveolar rhabdomyosarcoma. *Mol Carcinog* 2012;**51**:807–15.
20. Livak KJ, Schmittgen TD. Analysis of relative gene expression data using real-time quantitative PCR and the 2(-Delta Delta C(T)) Method. *Methods* 2001;**25**:402–8.
21. Gryder BE, Yohe ME, Chou HC, Zhang X, Marques J, Wachtel M, Schaefer N, Sen N, Song Y, Gualtieri A, Pomella S, Rota R, Cleveland A, Wen X, Sindiri S, Wei JS, Barr FG, Das S, Andresson T, Guha R, Lal-Nag M, Ferrer JF, Shern JF, Zhao K, Thomas CJ, Khan J. PAX3-FOXO1 Establishes Myogenic Super Enhancers and Confers BET Bromodomain Vulnerability. *Cancer Discov* 2017;**7**:884–99.
22. Zhang Y, Liu T, Meyer CA, Eeckhoute J, Johnson DS, Bernstein BE, Nusbaum C, Myers RM, Brown M, Li W, Liu XS. Model-based analysis of ChIP-Seq (MACS). *Genome Biol* 2008;**9**:R137.
23. Griffiths EA, Choy G, Redkar S, Taverna P, Azab M, Karpf AR. SGI-110: DNA Methyltransferase Inhibitor Oncolytic. *Drugs Future* 2013;**38**:535–43.
24. Kooistra SM, Helin K. Molecular mechanisms and potential functions of histone demethylases. *Nat Rev Mol Cell Biol* 2012;**13**:297–311.
25. Yamane K, Tateishi K, Klose RJ, Fang J, Fabrizio LA, Erdjument-Bromage H, Taylor-Papadimitriou J, Tempst P, Zhang Y. PLU-1 is an H3K4 demethylase involved in transcriptional repression and breast cancer cell proliferation. *Mol Cell* 2007;**25**:801–12.
26. Hyun K, Jeon J, Park K, Kim J. Writing, erasing and reading histone lysine methylations. *Exp Mol Med* 2017;**49** e324.
27. Babina IS, Turner NC. Advances and challenges in targeting FGFR signalling in cancer. *Nat Rev Cancer* 2017;**17**:318–32.
28. Porta R, Borea R, Coelho A, Khan S, Araujo A, Reclusa P, Franchina T, Van Der Steen N, Van Dam P, Ferri J, Sirera R, Naing A, Hong D, Rolfo C. FGFR a promising druggable target in cancer: Molecular biology and new drugs. *Crit Rev Oncol Hematol* 2017;**113**:256–67.
29. Tang S, Hao Y, Yuan Y, Liu R, Chen Q. Role of fibroblast growth factor receptor 4 in cancer. *Cancer Sci* 2018;**109**:3024–31.
30. Cao L, Yu Y, Bilke S, Walker RL, Mayeenuddin LH, Azorsa DO, Yang F, Pineda M, Helman LJ, Meltzer PS. Genome-wide identification of PAX3-FKHR binding sites in rhabdomyosarcoma reveals candidate target genes important for development and cancer. *Cancer Res* 2010;**70**:6497–508.
31. Musselman CA, Lalonde ME, Cote J, Kutateladze TG. Perceiving the epigenetic landscape through histone readers. *Nat Struct Mol Biol* 2012;**19**:1218–27.
32. Jeong KW, Kim K, Situ AJ, Ulmer TS, An W, Stallcup MR. Recognition of enhancer element-specific histone methylation by TIP60 in transcriptional activation. *Nat Struct Mol Biol* 2011;**18**:1358–65.
33. Flavahan WA, Drier Y, Johnstone SE, Hemming ML, Tarjan DR, Hegazi E, Shareef SJ, Javed NM, Raut CP, Eschle BK, Gokhale PC, Hornick JL, Sicinska GD, Demetri GD, Bernstein BE. Altered chromosomal topology drives oncogenic programs in SDH-deficient GISTs. *Nature* 2019;**575**:229–33.
34. Yang X, Han H, De Carvalho DD, Lay FD, Jones PA, Liang G. Gene body methylation can alter gene expression and is a therapeutic target in cancer. *Cancer Cell* 2014;**26**:577–90.
35. Liu M, Zhang L, Li H, Hinoue T, Zhou W, Ohtani H, El-Khoueiry A, Daniels J, O'Connell C, Dorff TB, Lu Q, Weisenberger DJ, Liang G. Integrative epigenetic analysis reveals therapeutic targets to the DNA methyltransferase inhibitor guadecitabine (SGI-110) in hepatocellular carcinoma. *Hepatology* 2018;**68**:1412–28.
36. Takebayashi S, Nakao M, Fujita N, Sado T, Tanaka M, Taguchi H, Okumura K. 5-Aza-2'-deoxycytidine induces histone hyperacetylation of mouse centromeric heterochromatin by a mechanism independent of DNA demethylation. *Biochem Biophys Res Commun* 2001;**288**:921–6.
37. Nguyen CT, Weisenberger DJ, Velicescu M, Gonzales FA, Lin JC, Liang G, Jones PA. Histone H3-lysine 9 methylation is associated with aberrant gene silencing in cancer cells and is rapidly reversed by 5-aza-2'-deoxycytidine. *Cancer Res* 2002;**62**:6456–61.
38. Gates LA, Foulds CE, O'Malley BW. Histone marks in the 'Driver's Seat': functional roles in steering the transcription cycle. *Trends Biochem Sci* 2017;**42**:977–89.
39. Clouaire T, Webb S, Skene P, Illingworth R, Kerr A, Andrews R, Lee JH, Skalnik D, Bird A. Cfp1 integrates both CpG content and gene activity for accurate H3K4me3 deposition in embryonic stem cells. *Genes Dev* 2012;**26**:1714–28.
40. Wysocka J, Swigut T, Milne TA, Dou Y, Zhang X, Burlingame AL, Roeder AH, Brivanlou AH, Allis CD. WDR5 associates with histone H3 methylated at K4 and is essential for H3 K4 methylation and vertebrate development. *Cell* 2005;**121**:859–72.
41. Dou Y, Milne TA, Ruthenburg AJ, Lee S, Lee JW, Verdine GL, Allis CD, Roeder RG. Regulation of MLL1 H3K4 methyltransferase activity by its core components. *Nat Struct Mol Biol* 2006;**13**:713–9.